

# Journal of Materials Chemistry C

Accepted Manuscript



This is an *Accepted Manuscript*, which has been through the Royal Society of Chemistry peer review process and has been accepted for publication.

*Accepted Manuscripts* are published online shortly after acceptance, before technical editing, formatting and proof reading. Using this free service, authors can make their results available to the community, in citable form, before we publish the edited article. We will replace this *Accepted Manuscript* with the edited and formatted *Advance Article* as soon as it is available.

You can find more information about *Accepted Manuscripts* in the [Information for Authors](#).

Please note that technical editing may introduce minor changes to the text and/or graphics, which may alter content. The journal's standard [Terms & Conditions](#) and the [Ethical guidelines](#) still apply. In no event shall the Royal Society of Chemistry be held responsible for any errors or omissions in this *Accepted Manuscript* or any consequences arising from the use of any information it contains.

# Preparation of Structurally Colored, Monodisperse Spherical Assemblies Composed of Black and White Colloidal Particles using a Micro Flow-Focusing Device

Midori Teshima<sup>1</sup>, Takahiro Seki<sup>1</sup>, Ryuji Kawano<sup>2,§</sup>, Shoji Takeuchi<sup>2,3</sup>, Shinya Yoshioka<sup>4\*</sup>, Yukikazu Takeoka<sup>1\*</sup>

<sup>1</sup>*Department of Molecular Design & Engineering, Nagoya University, Furo-cho, Chikusa-ku, Nagoya 464-8603, Japan*

<sup>2</sup>*Kanagawa Academy of Science and Technology, KSP EAST 303, 3-2-1, Sakado, Takatsu-ku, Kawasaki, Kanagawa 213-0012, Japan*

<sup>3</sup>*Institute of Industrial Science, The University of Tokyo, 4-6-1 Komaba, Meguro-ku, Tokyo 153-8505, Japan*

<sup>4</sup>*Graduate School of Frontier Biosciences, Osaka University, 1-3 Yamadaoka, Suita, Osaka 565-0871, Japan*

<sup>§</sup>*Present address: Division of Biotechnology and Life Science, Tokyo University of Agriculture and Technology, 2-24-16 Naka-cho Koganei-shi, Tokyo 184-8588, Japan*

[\*] Corresponding Author E-mail: ytakeoka@apchem.nagoya-u.ac.jp, syoshi@fbs.osaka-u.ac.jp

[\*\*] Y. T. acknowledges the support of Grants-in-Aid for Scientific Research (No. 23245047 and No. 22107012) on Innovative Areas: “Fusion Materials” (Area No. 2206) from the Ministry of Education, Culture, Sports, and Science (MEXT). S. Y. acknowledges the support of a Grant-in-Aid for Scientific Research (No. 24120004) on Innovative Areas: “Engineering Neo-Biomimetics” (Area No. 4402) from MEXT.

**Abstract**

It is very annoying when colors fade over time from exposure to bright light. Structurally colored material is a strong candidate for the fabrication of non-fading colored materials composed of environmentally friendly and non-toxic chemicals. We demonstrate that by using a micro flow-focusing device, monodisperse spherical assemblies displaying various structural colors in air can be prepared from a suspension containing environmentally friendly white and black colloidal particles: monodisperse submicron-sized SiO<sub>2</sub> colloidal particles and black magnetite colloidal particles. The average size of the monodisperse spherical assemblies can be controlled by changing the amount of SiO<sub>2</sub> colloidal particles used in the preparation of the suspension. The hue of the monodisperse spherical assemblies can be varied by simply altering the size of the SiO<sub>2</sub> colloidal particles. These monodisperse spherical assemblies exhibit either iridescent or non-iridescent structural colors, depending on the aggregation state of the SiO<sub>2</sub> colloidal particles, which can be controlled by the presence or absence of an electrolyte. Moreover, the saturation of the colors produced by the monodisperse spherical assemblies can be altered by modifying the amount of magnetite colloidal particles that is added. Our results should offer new possibilities for structurally colored materials for future application in pigments and test agents.

**Key words:** Structural Color, Colloidal Crystal, Colloidal Amorphous Array, Monodisperse Spherical Assembly, White and Black Particles

## 1. Introduction

The fabrication of non-fading and inexpensive colored materials composed of environmentally friendly and safe chemicals is expected to contribute to future sustainable and lasting developments. Structurally colored materials represent strong candidates for this purpose.<sup>1-4</sup> In general, structural colors originate from the interference, scattering, and diffraction of light from microstructured materials. The color tint is affected by the microscopic structural form of the materials and their refractive indices. For example, aggregations composed of monodisperse submicron-sized particles (hereafter referred to as “colloidal particles”) exhibit different structural colors depending on the microscopic ordered structures of the aggregations and their average refractive indices.<sup>5</sup> One of the most widely recognized types of aggregations of colloidal particles is a colloidal crystal film with a periodic optical nanostructure, which causes optical interference and results in a wavelength-selective reflection. Because the wavelength of optical interference depends on the viewing and illumination angles, a colloidal crystal film generally exhibits a glossy angle-dependent structural color.<sup>6-12</sup> Recently, it has emerged that colloidal amorphous array films composed of colloidal particles also exhibit structural color but with a low angle dependence.<sup>13-23</sup> In the past two decades, these membrane assemblies of colloidal particles have been the subject of extensive studies concerning their application in energy-saving displays and colorimetric sensors using the various optical characteristics of the assemblies. Currently, with the advancement of technologies for the preparation of colloidal assemblies, not only membrane assemblies but also assemblies of various other shapes and sizes can be prepared.<sup>5, 24, 25</sup> Among these assemblies, spherical assemblies (SAs) of colloidal particles have received considerable attention because of their possibilities in the development of dispersible structurally colored materials that may serve as the basis for non-fading pigments and test agents.<sup>22, 26-33</sup> For test agents using suspension arrays, a large number of spectral codes are required to obtain multiplex assay system. To use an SA for such applications, a monodisperse SA displaying various colors is preferred.<sup>34</sup> In previous reports, most SAs exhibiting structural color have been colloidal crystalline states.<sup>24, 30</sup> In addition, previously investigated SAs

can exhibit bright colors in solvents but turn white in air. This is because there is the large contribution of the incoherent multiple scattering of light that comes from imperfections of the crystalline structure. For structurally colored SAs to be used as replacements for traditional pigments and colored test agents, these SAs must satisfy various requirements, such as angle dependence or independence in the hue, saturation, and brightness, depending on their intended use. Thus, there is a plenty room for the investigation of SAs that are brightly colored even in air.

In this study, we produced several types of monodisperse SAs composed of monodisperse submicron-sized silica colloidal particles (hereafter referred to as “SiO<sub>2</sub> colloidal particles”) and black magnetite (Fe<sub>3</sub>O<sub>4</sub>) colloidal particles using a micro flow-focusing device (MFFD). It is shown that these SAs can display saturated colors even in the dried stated. Iridescent and non-iridescent brightly colored SAs were also prepared by the absence and presence of electrolyte. These newly prepared variously structural-coloured monodisperse SAs can be environmentally friendly and non-fading pigments, and may have potential applications in various fields.

## 2. Results and Discussion

SiO<sub>2</sub> colloidal particles were used as the main colloidal particles in this study. An MFFD (Figure 1a) composed of poly(methyl methacrylate) was used to prepare the monodisperse SAs of the SiO<sub>2</sub> colloidal particles.<sup>35</sup> We prepared the MFFD, which had a flow-focusing geometry of 100 μm integrated into a planar flow channel of 200 μm in diameter, such that the flow would form a w/o emulsion, with monodisperse aqueous liquid drops containing the SiO<sub>2</sub> colloidal particles in a continuous and immiscible oil phase (Figure 1b).<sup>36</sup> The oil phase consisted of hexadecane, including 2 wt% Span 80 surfactant. The aqueous and oil fluids were separately introduced into the MFFD using flexible silicon tubes, and the flow rates were controlled using separate syringe pumps for each fluid. The aqueous flow rate and oil flow rate that were injected into the MFFD were 2.1 μL/sec and 84 μL/sec, respectively. Figure 1b illustrates the moment of formation of a monodisperse aqueous liquid drop in the flow-focusing geometry implemented in the MFFD. An

aqueous liquid flows through the left-hand channel, and an immiscible oil liquid flows through the two channels above and below. The two liquid phases are forced to flow through a small orifice. Thus, monodisperse aqueous liquid drops that contain SiO<sub>2</sub> colloidal particles are continuously formed at the orifice. Previous studies of the preparation of monodisperse aqueous liquid drops in an immiscible oil fluid using flow-focusing methods in microfluidic devices have revealed that the droplet formation is determined by the balance between the shear and interfacial forces.<sup>37</sup> Furthermore, it is known that a liquid that is forced through an orifice into an immiscible fluid ultimately breaks up into drops because of surface tension through one of two mechanisms: dripping formation or jetting formation.<sup>38,39</sup> Judging from our experimental conditions and observations, the monodisperse aqueous liquid drops formed in the dripping regime in this experiment. The w/o emulsion containing the monodisperse aqueous liquid drops was poured directly into hexadecane with 2 wt% Span 80 surfactant in a PFA Petri dish on a hot plate at approximately 70°C (Figure 1c). The static standing monodisperse aqueous liquid drops poured into the oil phase did not coalesce in the Petri dish (Figure 1d). In Figure 2a, the drop diameter is plotted as a function of the concentration of the SiO<sub>2</sub> colloidal particles in the aqueous liquid. The concentration of the SiO<sub>2</sub> colloidal particles in the aqueous liquid slightly affected the size of the droplets, which may have been caused by the change in the surface tension of the droplets. A key factor in droplet size is the surface tension between the continuous and dispersive phases. It is known that the droplet size decreases as the interfacial tension decreases. The air-liquid surface tension of aqueous colloidal particle suspension increases with the colloidal particle concentration, because the Van der Waals force between particles at the interface increases surface free energy and thus increases surface tension. Therefore, as the interfacial tension at the oil-aqueous suspension must increase with the concentration of SiO<sub>2</sub> colloidal particles, the size of the droplet becomes larger.

After the application of heat to the aqueous liquid drops in the oil phase, monodisperse SAs of the SiO<sub>2</sub> colloidal particles were obtained in the oil. After the SAs were washed with hexane

several times, and dried in air, dried monodisperse SAs of the SiO<sub>2</sub> colloidal particles were obtained. The SAs are stable as the dried states even four years after the preparation. The SAs look white at a low magnification (Figure 2b-e), but they exhibit strong glossy reflection as shown later. We confirmed that monodisperse SAs were obtained regardless of the concentration of the SiO<sub>2</sub> colloidal particles because the coefficients of variation of the diameter of all SAs were lower than 10 % (Figure S2). The average size of the SAs could be increased by increasing the concentration of the SiO<sub>2</sub> colloidal particles, which were the main component in the aqueous solutions (Figure 2b-e). An increase in the concentration of the SiO<sub>2</sub> colloidal particles in the aqueous liquid drop caused the size of the SA to increase. We examined the aggregation states of the SiO<sub>2</sub> colloidal particles in the SAs using a scanning electron microscope (SEM). On the surface of the glossy SA, the SiO<sub>2</sub> colloidal particles were regularly arranged as shown in Figure 2f. Two-dimensional (2D) fast Fourier transform (FFT) analysis confirmed the hexagonally arranged sharp peaks in the power spectrum (inset of Figure 2f) indicating the presence of long-range positional order of the SiO<sub>2</sub> colloidal particles. Namely, the SAs were spherical colloidal crystals. The crystalline structure of the SiO<sub>2</sub> colloidal particles was also confirmed for the inner structure of the SAs by the cross sectional observation shown in Figure 2g.

The surface of the glossy SAs was sufficiently smooth to permit a ring-shaped light to be reflected from the surface into a microscope using white light. Under the directional light of the microscope, the ring-shaped specular color that was reflected by the SAs composed of 250-nm and 310-nm SiO<sub>2</sub> colloidal particles appeared to be blue-green and red, respectively (Figures 3a and 3b). Several previous studies have reported that colloidal crystal SAs composed of fine colloidal particles exhibit angle-independent properties in their transmission spectra and in coaxial measurements of their reflection spectra. This is because in the coaxial configuration the spectra of the SAs were measured under the same Bragg conditions and were therefore independent of the measurement angle.<sup>24-26</sup> However, in fact, the hues of the ring-shaped specular colors change depending on the viewing direction while the irradiation angle is fixed.<sup>32</sup> Thus, the scattering

spectra of the SAs were measured by changing only the detection angle while the incidence angle remained fixed (Figure 3c). The SAs were immobilized on the surface of a black carbon tape attached to a flat cover glass. The incidence angle relative to the normal of the planar surface of the cover glass was  $0^\circ$ . The detection angle,  $\theta$ , was varied from  $10^\circ$  to  $60^\circ$  relative to the normal of the planar surface of the cover glass. Figures 3d and 3e present the scattering spectra of each SA for various detection angles. We observed spectral peaks at 504 nm and 672 nm at  $\theta=10^\circ$  for the scattering spectra of the SAs composed of 250-nm and 310-nm SiO<sub>2</sub> colloidal particles, respectively. The intensity of these peaks did not change drastically with the detection angle, whereas the positions of the peaks shifted toward shorter wavelengths with increasing detection angle as shown in Figure 4. In the case of a colloidal crystal film, the Bragg reflection peak in the scattering spectrum disappears when the detection angle is deviated from the specular direction.<sup>17</sup> For a SA with a colloidal crystal structure, however, there is always a part of the sphere where the incident light is specularly reflected toward the observation direction. Thus, a Bragg reflection is thought to occur and produce a reflectance peak for any observation direction unlike a case of a flat crystal film. We analyzed the angular dependence to examine this hypothesis. From the hexagonal arrangement of the colloidal particles observed on the surface of SA (Figure 2f), we can reasonably assume that SA has the close-packed structure. The layer spacing  $d$  that causes Bragg reflection is related with the radius  $r$  of the colloidal particle by the following equation,

$$d = \frac{2\sqrt{6}}{3}r. \quad (1)$$

The wavelength  $\lambda$  that satisfies the Bragg condition is expressed as

$$\lambda = 2n_e d \cos \phi, \quad (2)$$

where  $n_e$  is the effective refractive index of SA and the refraction angle  $\phi$  is related to the incidence angle  $\phi_a$  in air by Snell's law  $\sin \phi_a = n_e \sin \phi$  with an assumption that the refractive index of air is unity. In the experimental geometry shown in Figure 3c, the incidence angle  $\phi_a$  corresponds to the half of the detection angle  $\theta$ . With these relations, it is found that the observed

peak-wavelength shift is reasonably reproduced as shown in Figure 4 with the parameters of  $2r = 310$  nm and  $n_e = 1.33$ , which is calculated as the volume average of refractive indices of air and SiO<sub>2</sub> (1.44) assuming the volume fraction 0.74 of the close-packed structure. From the reasonable matching, we can conclude that the observed spectral peak is attributed to the Bragg reflection.

In addition to the spectral peak, the scattering spectra presented in Figures 3d and 3e have a background-like component across the entire visible region that gradually increases with decreasing wavelength. This indicates that the incoherent multiple light scattering was strong enough to be comparable with the Bragg reflection peaks. This background-like component significantly affected the saturation of the perceived color because the component made the SAs appear white to the naked eye. The incoherent multiple scattering of light from the dried SAs can be attributed to the presence of defects in the crystal structure.<sup>21, 31, 32</sup> However, liquid immersion can drastically change the appearance of the SAs. Decreasing the refractive-index contrast reduced the multiple scattering of light and caused the SAs to appear transparent in toluene.<sup>13, 40</sup> Moreover, the ring-shaped blue-green portion of the SA composed of 250-nm SiO<sub>2</sub> colloidal particles turned bright green (Figure 3f), whereas the ring-shaped red portion of the SA composed of 310-nm SiO<sub>2</sub> colloidal particles disappeared (Figure 3g). Because the air between SiO<sub>2</sub> colloidal particles was replaced with toluene, which has a higher refractive index of 1.47 than air, the Bragg reflection occurred at a longer wavelength. In most previous studies, the brilliant structural colors of SAs have been observed under such conditions. We can notice in Figure 3f that not only the ring-shaped portion but also other regions appear bright green. This fact suggests that the colloidal crystal structure of the SAs is not a single crystal that spreads over the entire sphere but the crystal is separated into several or many domains with different crystal orientations. The observed bright region may correspond to a crystal domain that satisfies the Bragg condition in the experimental conditions.

Reduction of the incoherent scattering is necessary to make the SAs have saturated colors.

We successfully prepared such SAs by adding a small amount of black colloidal particles to the suspension of SiO<sub>2</sub> colloidal particle. In this experiment, magnetite colloidal particles were used as the black colloidal particles. The monodisperse aqueous liquid drops that contained the SiO<sub>2</sub> colloidal particles and the magnetite colloidal particles were gray or black in color immediately following their preparation using the MFFD. Figures 5a and 5b shows that the prepared SAs were colored blue and red, which were composed of 250-nm or 310-nm SiO<sub>2</sub> colloidal particles, respectively, with a small amount of magnetite colloidal particles (1 wt% in the aqueous fluid). Figures 5c and 5d present the scattering spectra of the SAs that were recorded when the measurement angle,  $\theta$ , was varied from 10° to 60° relative to the incidence angle. The position of the peak shifted toward shorter wavelengths with increasing detection angle similarly to the case of the SAs without magnetite colloidal particles (Figure 2d and e). However, the overall magnitude of the reflectance decreased with the incorporation of the magnetite colloidal particles, whereas the intensity of the peak component did not decrease significantly.

The polarization-dependent scattering spectra<sup>41</sup> of the SAs were measured to investigate the light-scattering processes occurring inside the SAs. The spectra were obtained using the methods described in Figure S5. White light was passed through a linear polarizer before being used to illuminate the SAs. The incidence angle relative to the normal of the planar surface of the cover glass where the SAs were immobilized was 0°. The polarization of the incident light was parallel to the scattering plane containing the incident beam and detector. The detector was placed at a fixed angle of 10° to the surface normal. Another linear polarizer was placed in front of the detector, and the direction of polarization was adjusted to be either parallel (co-polarization) or perpendicular (cross-polarization) to the scattering plane. Figure 5e presents the polarization-dependent scattering spectra of the SAs composed of 310-nm SiO<sub>2</sub> colloidal particles with and without magnetite colloidal particles. In the spectrum of the co-polarized light scattered from the SAs, a distinct spectral peak was observed at approximately 670 nm, regardless of whether the magnetite colloidal particles were present. These peaks were attributed to the Bragg reflection

of light caused by the presence of the crystalline structure of the SiO<sub>2</sub> colloidal particles. In the cross-polarized light spectrum for the SA composed of only the SiO<sub>2</sub> colloidal particles, no apparent peak could be observed; however, there was a background-like component throughout the entire visible region (Figure 5e). Because the depolarized spectrum can include high-order scattering, multiple and incoherent light scattering from the SiO<sub>2</sub> colloidal particles was thought to cause the background-like component. When the SA contains black materials, such as magnetite, they absorb more light that dwells longer inside the SA. Thus, the background component could be reduced by the addition of the black magnetite colloidal particles. As a result, the contribution of the Bragg reflection became more prominent<sup>31</sup>, and consequently, the structural colors became more saturated.

We could also produce spherical assemblies with different reflective properties when phenyl trimethyl ammonium chloride was added to the aqueous phase to serve as an electrolyte;<sup>13,32</sup> the produced SAs composed of SiO<sub>2</sub> colloidal particles and a small amount of magnetite colloidal particles exhibited matte structural colors lacking the ring-shaped specular reflection (Figure 6a). An electron micrograph showed that the arrangement of the SiO<sub>2</sub> colloidal particles looked random on the surface (Figure 6b), and the circular pattern (inset of Figure 6b) near the origin in the 2D FFT confirms the presence of only short-range order.<sup>42</sup> Thus, the microstructure of the aggregation was isotropic and amorphous. The amorphous aggregation state was confirmed also in their interior structure (Figure 6c). Such an aggregation state could be realized upon the addition of the electrolyte because the presence of the electrolyte caused the repulsive force between the SiO<sub>2</sub> colloidal particles to diminish,<sup>43</sup> thereby allowing the SiO<sub>2</sub> colloidal particles to form an amorphous array. The scattering peaks of the matte SA composed of 310-nm SiO<sub>2</sub> colloidal particles were considerably broader than those of the SAs with a crystalline structure (Figure 6d). Such a broad peak is characteristic to a colloidal amorphous array. The position of the peak is nearly independent of the detection angle partly because of the isotropic microstructure of colloidal amorphous arrays.

Finally, we compare the dependence of the peak wavelength on the detection angle in the scattering spectra of the glossy and matte SAs (prepared with or without an electrolyte,

respectively) composed of only 310-nm SiO<sub>2</sub> colloidal particles. We used the experimental configuration illustrated in Figure 3c. Figure 4 includes the peak wavelength shift observed for the matt SAs. The peak shift of the glossy SAs can be explained by the Bragg reflection (Eq. 2) because there is a part of the sphere that satisfies the Bragg condition for any observation direction. On the other hands, the peak wavelength observed in the scattering spectra of the matte SA appeared to remain largely unchanged with increasing  $\theta$ . This peak is considered to originate from constructive interference caused by the short-range order, and its less angle dependence is known to be characteristic to an amorphous array having an isotropic structure.

### 3. Conclusion

In conclusion, using an MFFD, we were able to prepare several sizes of stable monodisperse SAs that exhibited various colors depending on the concentration of the SiO<sub>2</sub> colloidal particles, the size of the SiO<sub>2</sub> colloidal particles, the amount of magnetite colloidal particles, and the presence or absence of an electrolyte in the aqueous phase<sup>[25]</sup>. The size of the monodisperse SAs could be controlled by changing the concentration of SiO<sub>2</sub> colloidal particles present in the aqueous phase. We demonstrated that the hue of the SAs could be varied by simply altering the size of the SiO<sub>2</sub> colloidal particles. The addition of magnetite colloidal particles to the aqueous phase made the SAs to have more saturated structural colors even in the dried state. We could change the aggregation states of the SiO<sub>2</sub> colloidal particles in the SAs through the presence or absence of an electrolyte. A glossy and iridescent SA was obtained in the absence of an electrolyte, whereas a matte and non-iridescent SA was prepared in the presence of an electrolyte.

Because various types of stable monodisperse spherical, structurally colored particles composed of white and black, safe and environmentally friendly components could be produced using an MFFD, such assemblies are promising for the future development and manufacture of non-fading pigments with low toxicity and minimal environmental impact. Our structurally colored SAs can also be used to prepare novel test agents, such as bar codes, that display various colors;

such test agents may eventually become an essential part of our healthcare system. This newly prepared, brightly and variously structural-coloured SAs may also have potential applications in various fields where highly toxic heavy-metal-containing pigments are used.

#### 4. Experimental Section

##### Materials

Fine spherical SiO<sub>2</sub> colloidal particles (Nippon Shokubai KE-P20, with an average diameter of 250 nm, and KE-W30, with an average diameter of 310 nm), magnetite colloidal particles (FerroTec EMG 1111, with an average diameter of 10 nm), hexadecane (Tokyo Chemical Industry, Co., Ltd.), Span 80 (Tokyo Chemical Industry, Co., Ltd.), and phenyl trimethyl ammonium chloride (Tokyo Chemical Industry, Co., Ltd.) for use as an electrolyte were purchased and used as received. Deionized water with a resistivity of 18.2 mΩ was used to perform all the experiments.

##### Preparation of MFFD

The flow channel of the MFFD was fabricated by machining a 1.5-mm-thick, 2 cm × 3 cm PMMA plate using a CAD/CAM 3-D modeling machine (MM-100, Modia Systems, Japan) with positioning accuracy of 6 μm. A flat PMMA plate of the same size was glued to the processed PMMA plate under thermal pressure at 120°C and  $5 \times 10^5$  N/m<sup>2</sup> for 20 min. Fittings (VRM 106, ISIS Co., Ltd.) were attached to each flow channel for the injection of the fluids from outside. Microsyringes (Hamilton, 1 mL) with oil and aqueous fluids were connected to the MFFD via silicone tubes with 1-mm inner diameters (LABOLAN). Syringe pumps (Elite Nano Mite, Harvard Apparatus, USA) were used to control the fluid flow.

##### Preparation of SAs

The preparation procedure for the SAs is described in the main text.

## Measurements

A UV-Vis spectrometer (Nippon Bunko Company, V-670) with an absolute reflectance measurement unit (ARMN-735) was used to measure the scattering spectra. The arrangements of the SiO<sub>2</sub> colloidal particles in the arrays were investigated using a scanning electron microscope (SEM, Hitachi, Miniscope TM3000). The samples were coated with a 10-nm Au-Pd layer using a magnetron sputtering apparatus (MSP-1S), and the images were obtained using the SEM operated at 15 kV. Photographs showing the structural colors of the samples were acquired using a digital camera and a digital microscope (KEYENCE VHX-500).

## Acknowledgments

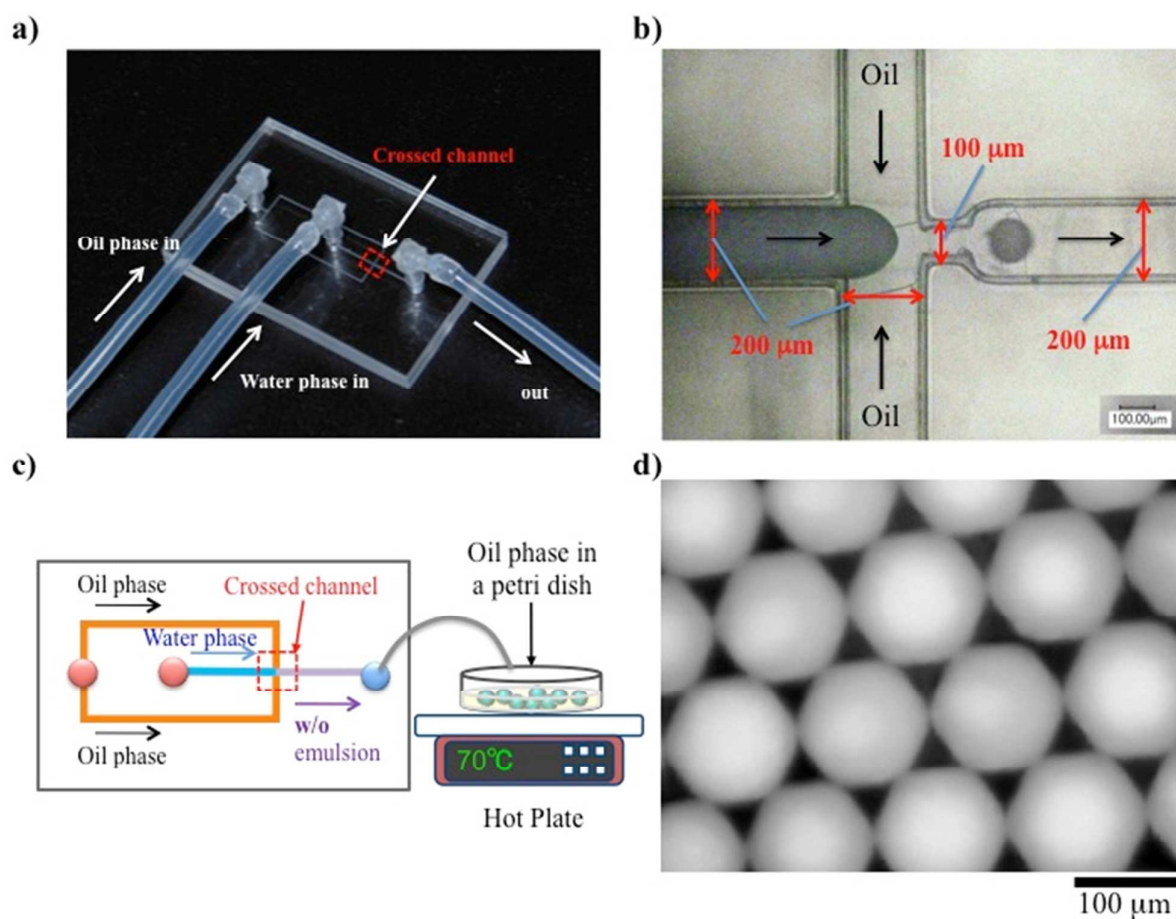
This work was supported by Grants-in-Aid for Scientific Research (No. 23245047, No. 22340121, No. 22107012, and No. 24120004) on the Innovative Areas of "Fusion Materials" (Area No. 2206) and "Engineering Neo-Biomimetics" (Area No. 4402) from the Ministry of Education, Culture, Sports, Science and Technology (MEXT).

## References

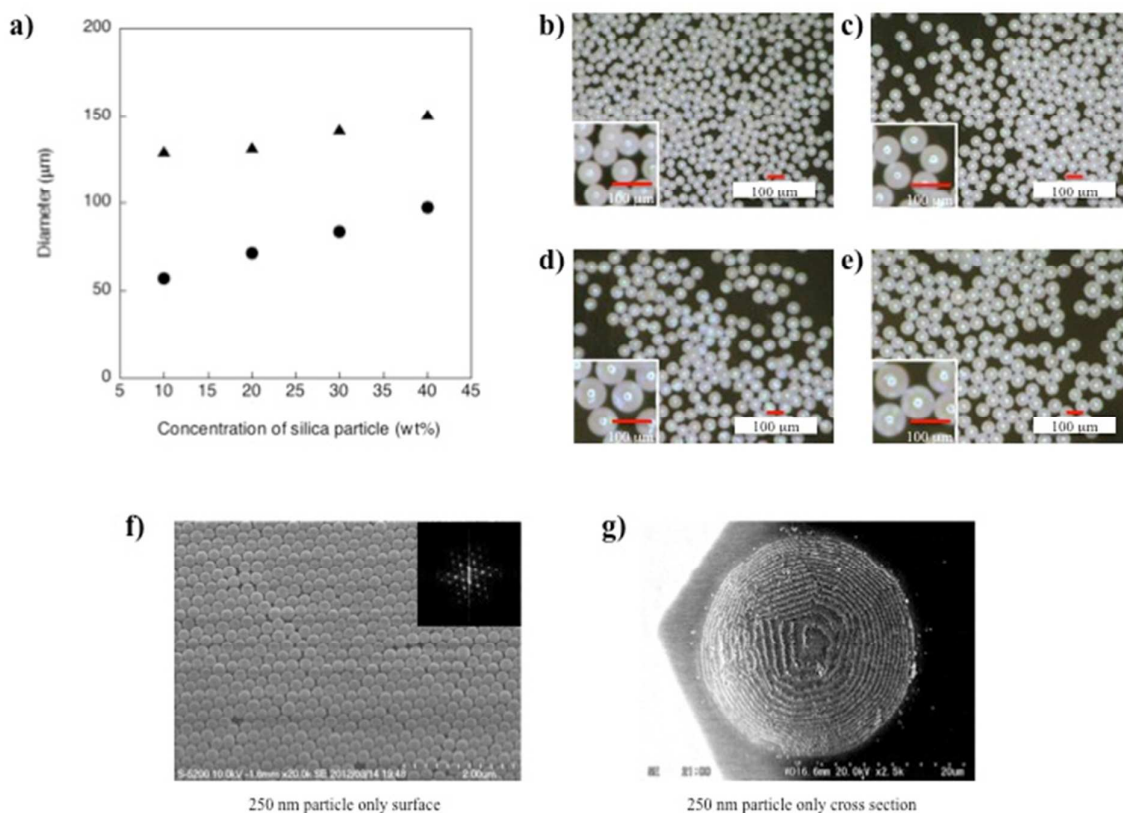
1. S. Kinoshita and S. Yoshioka, *ChemPhysChem*, 2005, **6**, 1442-1459.
2. M. Srinivasarao, *Chem Rev*, 1999, **99**, 1935-1961.
3. A. R. Parker, *J Opt a-Pure Appl Op*, 2000, **2**, R15-R28.
4. P. Vukusic and J. R. Sambles, *Nature*, 2003, **424**, 852-855.
5. Y. Takeoka, *J Mater Chem C*, 2013, **1**, 6059-6074.
6. H. Miguez, F. Meseguer, C. Lopez, A. Blanco, J. S. Moya, J. Requena, A. Mifsud and V. Fornes, *Adv Mater*, 1998, **10**, 480-483.
7. H. Miguez, N. Tetreault, S. M. Yang, V. Kitaev and G. A. Ozin, *Adv Mater*, 2003, **15**, 597-600.
8. H. Fudouzi and Y. N. Xia, *Adv Mater*, 2003, **15**, 892-896.
9. S. H. Park, B. Gates and Y. N. Xia, *Adv Mater*, 1999, **11**, 462-466.
10. C. I. Aguirre, E. Reguera and A. Stein, *Advanced Functional Materials*, 2010, **20**,

- 2565-2578.
11. F. Marlow, Muldarisnur, P. Sharifi, R. Brinkmann and C. Mendive, *Angew Chem Int Edit*, 2009, **48**, 6212-6233.
  12. J. P. Ge and Y. D. Yin, *Angew Chem Int Edit*, 2011, **50**, 1492-1522.
  13. M. Harun-Ur-Rashid, A. Bin Imran, T. Seki, M. Ishi, H. Nakamura and Y. Takeoka, *Chemphyschem*, 2010, **11**, 579-583.
  14. Y. Gotoh, H. Suzuki, N. Kumano, T. Seki, K. Katagiri and Y. Takeoka, *New J Chem*, 2012, **36**, 2171-2175.
  15. L. Shi, Y. F. Zhang, B. Q. Dong, T. R. Zhan, X. H. Liu and J. Zi, *Adv Mater*, 2013, **25**, 5314-5320.
  16. Y. Takeoka, *Journal of Photopolymer Science and Technology*, 2009, **22**, 123-132.
  17. R. Hirashima, T. Seki, K. Katagiri, Y. Akuzawa, T. Torimoto and Y. Takeoka, *J Mater Chem C*, 2014, **2**, 344-348.
  18. J. K. Yang, C. Schreck, H. Noh, S. F. Liew, M. I. Guy, C. S. O'Hern and H. Cao, *Physical Review A*, 2010, **82**.
  19. S. F. Liew, J. Forster, H. Noh, C. F. Schreck, V. Saranathan, X. Lu, L. Yang, R. O. Prum, C. S. O'Hern, E. R. Dufresne and H. Cao, *Optics Express*, 2011, **19**, 8208-8217.
  20. S. F. Liew, J. K. Yang, H. Noh, C. F. Schreck, E. R. Dufresne, C. S. O'Hern and H. Cao, *Physical Review A*, 2011, **84**.
  21. J. D. Forster, H. Noh, S. F. Liew, V. Saranathan, C. F. Schreck, L. Yang, J. G. Park, R. O. Prum, S. G. J. Mochrie, C. S. O'Hern, H. Cao and E. R. Dufresne, *Adv Mater*, 2010, **22**, 2939-2944.
  22. D. T. Ge, L. L. Yang, G. X. Wu and S. Yang, *J Mater Chem C*, 2014, **2**, 4395-4400.
  23. S. Yoshioka and Y. Takeoka, *ChemPhysChem*, 2014, **15**, 2209-2215.
  24. S. H. Kim, S. H. Kim and S. M. Yang, *Adv Mater*, 2009, **21**, 3771-3775.
  25. M. X. Kuang, J. X. Wang, B. Bao, F. Y. Li, L. B. Wang, L. Jiang and Y. L. Song, *Adv Opt Mater*, 2014, **2**, 34-38.
  26. J. H. Moon, G. R. Yi, S. M. Yang, D. J. Pine and S. Bin Park, *Adv Mater*, 2004, **16**, 605-+.
  27. S. H. Kim, S. J. Jeon, W. C. Jeong, H. S. Park and S. M. Yang, *Adv Mater*, 2008, **20**, 4129-4134.
  28. O. D. Velev, A. M. Lenhoff and E. W. Kaler, *Science*, 2000, **287**, 2240-2243.
  29. V. Rastogi, S. Melle, O. G. Calderon, A. A. Garcia, M. Marquez and O. D. Velev, *Adv Mater*, 2008, **20**, 4263-4268.
  30. Y. J. Zhao, X. W. Zhao, C. Sun, J. Li, R. Zhu and Z. Z. Gu, *Analytical Chemistry*, 2008, **80**, 1598-1605.

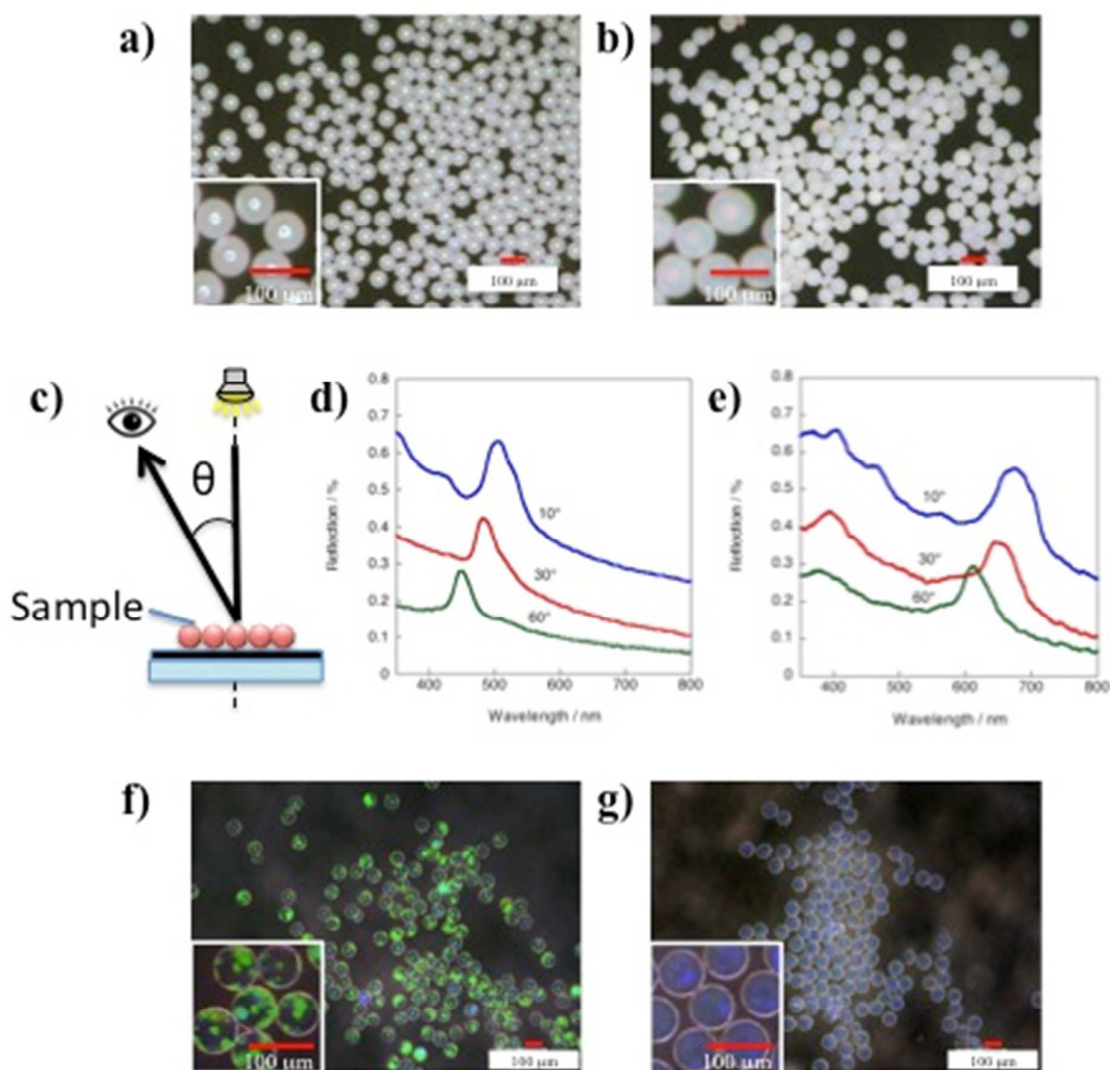
31. Y. Takeoka, S. Yoshioka, A. Takano, S. Arai, K. Nueangnoraj, H. Nishihara, M. Teshima, Y. Ohtsuka and T. Seki, *Angew Chem Int Edit*, 2013, **52**, 7261-7265.
32. Y. Takeoka, S. Yoshioka, M. Teshima, A. Takano, M. Harun-Ur-Rashid and T. Seki, *Sci Rep-Uk*, 2013, **3**.
33. J. G. Park, S. H. Kim, S. Magkiriadou, T. M. Choi, Y. S. Kim and V. N. Manoharan, *Angew Chem Int Edit*, 2014, **53**, 2899-2903.
34. G. R. Yi, V. N. Manoharan, S. Klein, K. R. Brzezinska, D. J. Pine, F. F. Lange and S. M. Yang, *Adv Mater*, 2002, **14**, 1137-1140.
35. S. Takeuchi, P. Garstecki, D. B. Weibel and G. M. Whitesides, *Adv Mater*, 2005, **17**, 1067-1072.
36. S. L. Anna, N. Bontoux and H. A. Stone, *Appl Phys Lett*, 2003, **82**, 364-366.
37. W. J. Lan, S. W. Li, J. H. Xu and G. S. Luo, *Langmuir*, 2011, **27**, 13242-13247.
38. C. Cramer, P. Fischer and E. J. Windhab, *Chem Eng Sci*, 2004, **59**, 3045-3058.
39. A. S. Utada, A. Fernandez-Nieves, H. A. Stone and D. A. Weitz, *Phys Rev Lett*, 2007, **99**.
40. Y. Takeoka, M. Honda, T. Seki, M. Ishii and H. Nakamura, *Acs Appl Mater Inter*, 2009, **1**, 982-986.
41. H. Noh, S. F. Liew, V. Saranathan, R. O. Prum, S. G. J. Mochrie, E. R. Dufresne and H. Cao, *Optics Express*, 2010, **18**, 11942-11948.
42. R. O. Prum, R. H. Torres, S. Williamson and J. Dyck, *Nature*, 1998, **396**, 28-29.
43. P. D. Garcia, R. Sapienza, A. Blanco and C. Lopez, *Adv Mater*, 2007, **19**, 2597-2602.



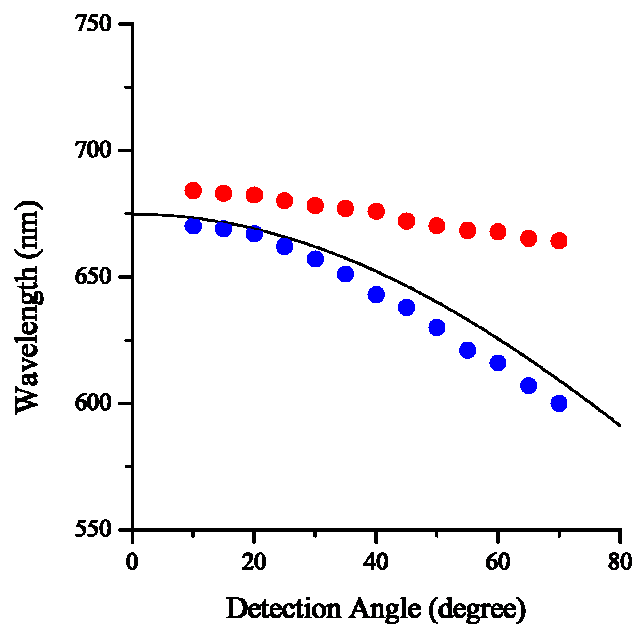
**Fig. 1** a) Our micro flow-focusing device (MFFD). b) Formation of a droplet at the crossed channel of the MFFD. c) Diagram of the SA preparation process. d) Monodisperse aqueous liquid drops in the oil phase.



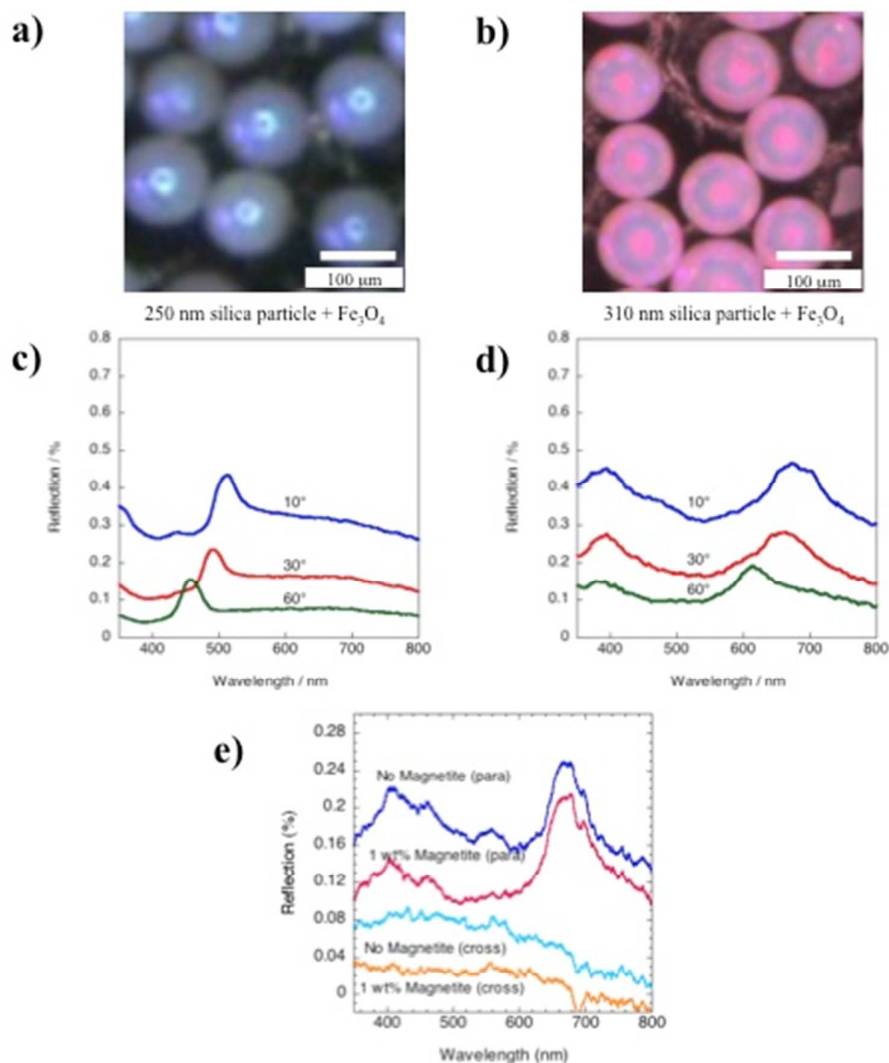
**Fig. 2** a) Plot showing the diameters of a monodisperse aqueous liquid drop, ▲, and an SA composed of 310-nm SiO<sub>2</sub> colloidal particles, ●, as functions of the concentration of the SiO<sub>2</sub> colloidal particles. b)-e) Images of dried SAs composed of 250-nm SiO<sub>2</sub> colloidal particles at various concentrations: b) 10 wt%, c) 20 wt%, d) 30 wt%, and e) 40 wt%. The insets present the magnified figures. f) A surface SEM image of a glossy SA composed of 250-nm SiO<sub>2</sub> colloidal particles. The inset presents the corresponding 2D FFT image. g) A cross-sectional SEM image of a glossy SA composed of 250-nm SiO<sub>2</sub> colloidal particles prepared by microtoming the embedded sample.



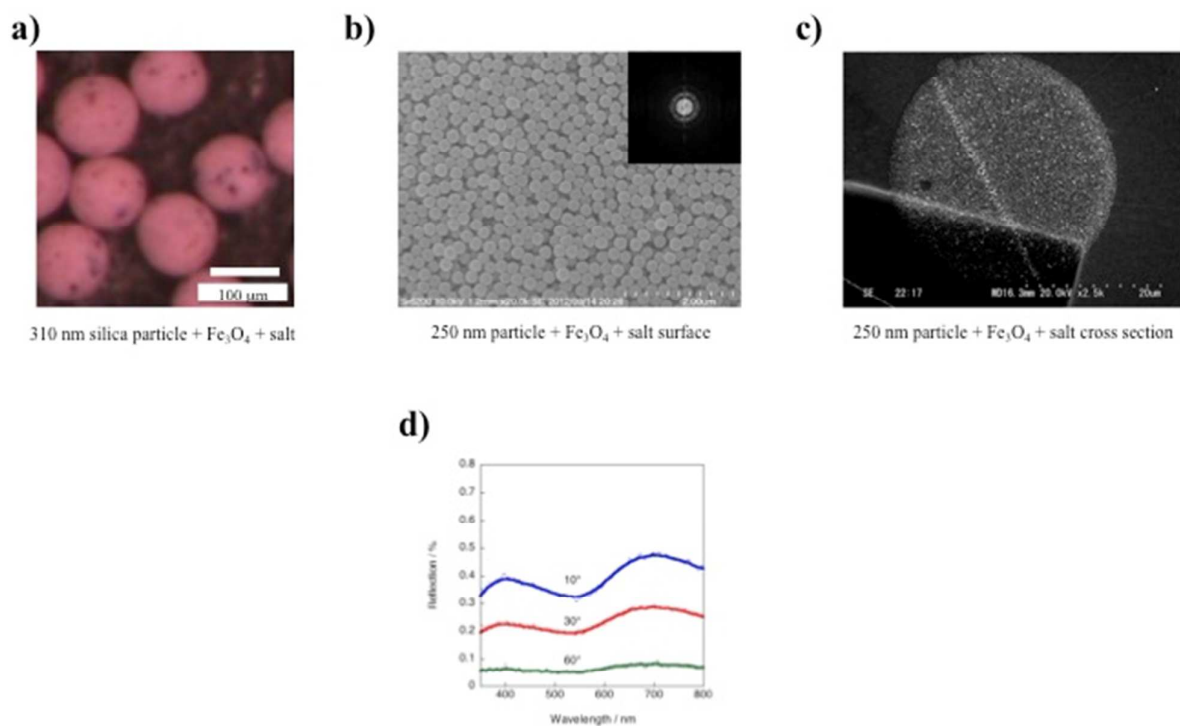
**Fig. 3** a) A glossy SA composed of 250-nm SiO<sub>2</sub> colloidal particles in air and b) a glossy SA composed of 310-nm SiO<sub>2</sub> colloidal particles in air. The insets present the magnified figures. c) Schematic diagram of the optical setup for the measurement of the diffusive scattering spectra of white light. The incidence angle relative to the normal of the planar surface of the glass plate was 0°. The measurement angle,  $\theta$ , was varied from 10° to 30° to 60° relative to the normal of the planar surface of the glass plate. d) Scattering spectra of a glossy SA composed of 250-nm SiO<sub>2</sub> colloidal particles, recorded at various measurement angles. e) Scattering spectra of a glossy SA composed of 310-nm SiO<sub>2</sub> colloidal particles, recorded at various measurement angles. f) A glossy SA composed of 250-nm SiO<sub>2</sub> colloidal particles in toluene. The inset presents the magnified figure. g) A glossy SA composed of 310-nm SiO<sub>2</sub> colloidal particles in toluene. The inset presents the magnified figure.



**Fig. 4** Plots showing the peak wavelengths of a glassy SA, ●, and a matte SA, ●, composed of 310-nm SiO<sub>2</sub> colloidal particles versus the detection angle. Black curve is theoretically drawn according to Eq. 2. See text for detail.

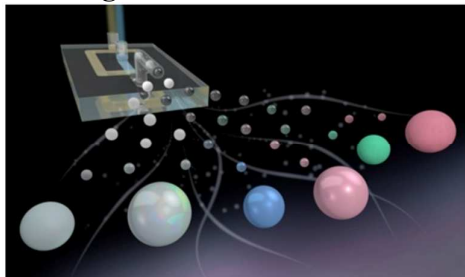


**Fig. 5** a) A saturated glossy SA composed of 250-nm SiO<sub>2</sub> colloidal particles (30 wt% in the aqueous fluid) and magnetite colloidal particles (1 wt% in the aqueous fluid) in air. b) A saturated glossy SA composed of 310-nm SiO<sub>2</sub> colloidal particles (30 wt% in the aqueous fluid) and magnetite colloidal particles (1 wt% in the aqueous fluid) in air. c) Scattering spectra of the glossy SA composed of 250-nm SiO<sub>2</sub> colloidal particles and magnetite colloidal particles, recorded at various measurement angles. d) Scattering spectra of the glossy SA composed of 310-nm SiO<sub>2</sub> colloidal particles and magnetite colloidal particles, recorded at various measurement angles. e) Co-polarization and cross-polarization reflection spectra of glossy SAs composed of 310-nm SiO<sub>2</sub> colloidal particles with and without magnetite colloidal particles: the solid blue line represents p-polarization without magnetite colloidal particles, the solid cyan line represents s-polarization without magnetite colloidal particles, the solid red line represents p-polarization with magnetite colloidal particles, and the solid orange line represents s-polarization with magnetite colloidal particles.



**Fig. 6** a) A saturated matte SA composed of 310-nm SiO<sub>2</sub> colloidal particles (30 wt% in the aqueous fluid) and magnetite colloidal particles (1 wt% in the aqueous fluid) in air. b) A surface SEM image of a matte SA composed of 250-nm SiO<sub>2</sub> colloidal particles. The inset presents the corresponding 2D FFT image. c) A cross-sectional SEM image of a matte SA composed of 250-nm SiO<sub>2</sub> colloidal particles prepared by microtoming the embedded sample. d) Scattering spectra of the matte SA composed of 310-nm SiO<sub>2</sub> colloidal particles and magnetite colloidal particles, recorded at various measurement angles.

TOC Figure



Monodisperse-spherical-assemblies displaying various structural-colors in air can be prepared by white and black colloidal particles using a micro flow-focusing device.